Research Article
Vol. 27, No. 16 | 5 Aug 2019 | OPTICS EXPRESS 22385
Optics EXPRESS

# Phase stabilization of an attosecond beamline combining two IR colors

F. SCHLAEPFER,[1,2,4] M. VOLKOV,[1,2,3,5] N. HARTMANN,[1] A. NIEDERMAYR,[1] Z. SCHUMACHER,[1] L. GALLMANN,[1] AND U. KELLER[1]

[1]*Department of Physics, ETH Zurich, 8093 Zurich, Switzerland*
[2]*These authors contributed equally to this work*
[3]*Current address: Ludwig-Maximilians-Universität München, 85748 Garching, Germany*
[4]*f.schlaepfer@phys.ethz.ch*
[5]*volkovm@phys.ethz.ch*

**Abstract:** We present a phase-stabilized attosecond pump-probe beamline involving two separate infrared wavelengths for high-harmonic generation (HHG) and pump or probe. The output of a Ti:sapphire laser is partly used to generate attosecond pulses via HHG and partly to pump an optical parametric amplifier (OPA) that converts the primary Ti:sapphire radiation to a longer wavelength. The attosecond pulse and down-converted infrared are recombined after a more than 20-m-long Mach-Zehnder interferometer that spans across two laboratories and separate optical tables. We demonstrate a technique for active stabilization of the relative phase of the pump and probe to within 450 as rms, without the need for an auxiliary continuous wave (cw) laser. The long-term stability of our system is demonstrated with an attosecond photoelectron streaking experiment. While the technique has been shown for one specific OPA output wavelength (1560 nm), it should also be applicable to other OPA output wavelengths. Our setup design permits tuning of the OPA wavelength independently from the attosecond pulse generation. This approach yields new possibilities for studying the wavelength-dependence of field-driven attosecond electron dynamics in various systems.



## 1. Introduction

Typically, attosecond beamlines combine a few-cycle infrared (IR) pulse with an attosecond extreme-ultraviolet (XUV) pulse in a pump-probe setup. The XUV radiation is produced from a primary IR beam via HHG. To date, most of the setups rely on a single IR wavelength for HHG and as a pump or probe in the experiment. The stability of the pump-probe delay represents a challenge for resolving sub-femtosecond dynamics. For example, a change of the relative path length between the pump and probe arms of the setup by 100 nm results in a delay offset by 330 as. Hence, the implementation of an active delay stabilization system can be crucial for enabling accurate attosecond measurements – in particular over extended measurement times [1–3].

An often adopted attosecond beamline design incorporates a Mach-Zehnder interferometer for the pump and probe beams [4,5]. A fraction of the IR laser beam is split off before the HHG target and later recombined with the generated XUV radiation via a center-hole mirror. In this case, the two arms of the interferometer extending from the beam splitter to the recombination point can be stabilized against each other using an auxiliary continuous wave (cw) laser. Delay stability within few tens of attoseconds has been demonstrated using this approach [1,3,6].

Recently, an experiment has emerged that involves two separate IR colors for HHG (1800 nm) and probe (800 nm) [7]. The XUV generated by the long-wavelength driver is recombined with the 800-nm pulse to perform a pump-probe experiment. Passive delay stability of this system was sufficient for resolving molecular dynamics on a time scale of few tens of femtoseconds. Improving the temporal resolution to the attosecond regime, however, requires active stabilization of the pump-probe delay.

#367488 https://doi.org/10.1364/OE.27.022385
Journal © 2019 Received 14 May 2019; revised 25 Jun 2019; accepted 6 Jul 2019; published 23 Jul 2019

Optics EXPRESS

In this paper, we present what is to our knowledge the first actively stabilized two-IR-color setup (780 nm, 1560 nm) with a sub-femtosecond temporal resolution. The use of an auxiliary, common-path cw laser is unpractical in a two-color beamline since an OPA system is installed in one of the pump-probe arms for the conversion of the primary Ti:sapphire beam to the desired longer wavelengths. Numerous dielectric and dichroic optics in the interferometer arms are an additional obstacle. Our approach, presented in detail below, actively stabilizes the phase between the two separate IR colors. The relative phase stability is essential to resolve ultrafast dynamics, since most attosecond measurement techniques, as the attosecond streak camera [8], extract the time information via a phase analysis of a pump/probe induced oscillation [9–12]. We demonstrate a long-term rms delay stability below 500 as despite the pump-probe interferometer arms having a length of approximately 23 m and spanning between two laboratories. We perform a proof-of-principle photoelectron streaking measurement to demonstrate the importance of the active stabilization. The stabilization approach should be applicable also for other OPA output wavelengths, as long as the second harmonic spectrum of the OPA partly overlaps with the shorter IR-wavelength.

Our beamline design allows for tuning of the photon energy of the IR pulse used in the pump-probe experiment without affecting the spectral shape of the generated XUV attosecond pulse. This will enable a frequency-dependent investigation of optical-field-induced carrier dynamics in condensed matter systems, such as the dynamical Franz-Keldysh effect [13,14].

## 2. Laser and pump-probe schemes

We use a commercial Ti:sapphire chirped-pulse-amplified (CPA) laser system providing near-infrared (NIR) pulses at a center wavelength of about 780 nm and operating at a repetition rate of 1 kHz. The carrier envelope offset phase (CEP [15]) is actively stabilized. A sketch of the experimental setup is shown in Fig. 1. The output beam of the CPA system propagates through a spatial beam cleaning system and is compressed with a combination of gratings and chirped mirrors to about 25 fs. The beam with a remaining energy of 7 mJ is divided into two parts. One part is used to pump an OPA, the other one generates attosecond high-harmonic radiation. The beam paths are described in detail below. The OPA output and attosecond pulse are finally recombined, comprising a 23-m-long Mach-Zehnder interferometer partly exposed to air and crossing between two rooms and two optical tables. The two beams are focused into the interaction chamber by a toroidal mirror. For our proof-of-principle measurement, the interaction chamber is equipped with a gas nozzle and a time-of-flight electron spectrometer. We use several beam pointing stabilization systems (MRC, Femtolasers) in the first room with the laser systems and an additional one (Thorlabs) for the routing of the two beams via an evacuated tube to the second room with the experimental chamber.

The path length from the CPA system to the OPA accumulates to several meters due to the particular space constraints of our laboratory. The peak power of the laser pulses after compression is around 250 GW and thus significantly exceeds the critical power for self-focusing in air (10 GW [16]). As a result, any beam inhomogeneity originating from the multi-pass CPA system can be rapidly amplified by the Kerr effect within a few meters of beam routing, leading to the formation of hot spots. To mitigate this, the CPA laser output is propagated through a spatial beam cleaning system, specially designed for high-peak-power radiation. Since the peak intensity of the focused beam after compression would exceed the breakdown threshold of any material, the beam cleaning system is placed before the grating compressor (Fig. 1). The beam is focused onto a Fourier-plane aperture mounted inside an evacuated tube. The spatial filter is a 3-mm long slice of a fused silica hollow-core fiber with an inner diameter of 420 μm. The focusing mirror has a radius of curvature of 4 m, which results in a nominal spot size of ~275 μm ($1/e^2$ beam width).

The cleaned and compressed beam is divided with an 85/15 beam splitter (BS) into two beam paths. The smaller fraction (15%) is further compressed using a filament compressor [4]. It is then guided through a polarization gating (PG [5]) setup and finally used for HHG in argon. Depending on the amount of pulse compression and the orientation of the birefringent crystals in the PG setup, either an attosecond pulse train (APT) or a single attosecond pulse (SAP) can be generated, both having a spectrum in the extreme-ultraviolet (XUV) energy regime. After the HHG gas target, a 100-nm-thick aluminum foil in the beam path filters out the residual NIR radiation.

The beam containing the 85% of the original laser output after reflection on the beam splitter is sent to an OPA from Light Conversion (HE-TOPAS prime). The output wavelength of the signal and idler of the OPA can be tuned between 1160-1600 nm and 1600-2600 nm, respectively. In the present study, we use the signal wavelength set at 1560 nm. To avoid confusion between the Ti:sapphire (780 nm) and TOPAS (1560 nm) outputs, we label them from now on as *NIR* and *OPA* beams. The OPA pulses have an energy of up to 630 µJ and a duration of approximately 40-45 fs. The OPA beam propagates further via a delay line equipped with a piezo-controlled stage and is finally recombined collinearly with the XUV radiation on the center-hole mirror, see Fig. 2(a).

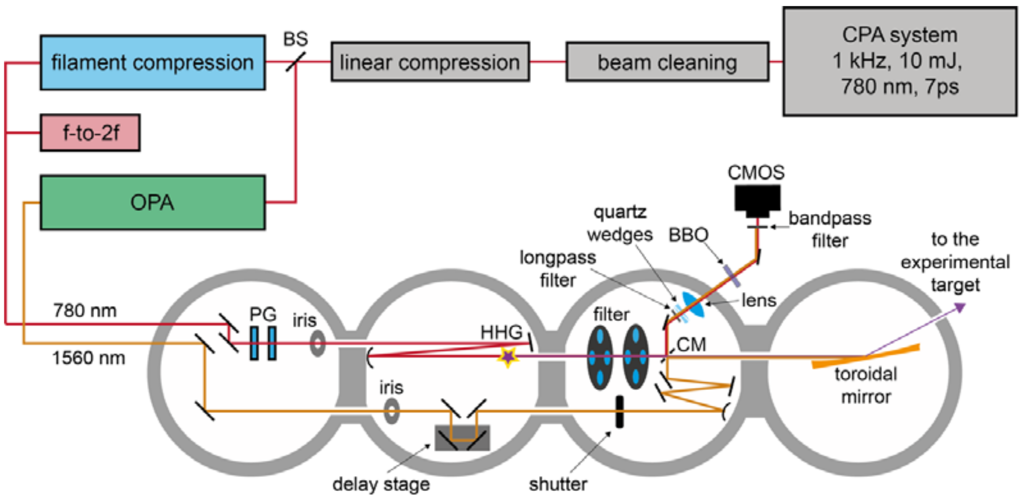


Fig. 1. Ti:sapphire laser system, OPA and pump-probe scheme. The beam profile of the CPA output is cleaned before the linear pulse compression. An f-to-2f interferometer installed after the nonlinear filament compression monitors slow CEP drifts of the NIR radiation and feeds an error signal to an actuator in a phase-locked loop. The interferometer spans from the beam splitter (BS) to the center-hole mirror (CM) used for recombination. The optics on the path toward the CMOS camera is described in detail in the text and Fig. 2.

## 3. Phase stabilization scheme

The established method of using an auxiliary cw laser to stabilize the pump-probe interferometer, as described in [1], is not possible due to the OPA being present in one of the arms and numerous incompatible dielectric and dichroic optics along the beam paths. In this section, we present our approach to directly stabilize the phase between the two IR colors without the need for any additional laser.

As illustrated in Fig. 2(a), we use an aluminum foil after the HHG target with a slightly smaller diameter than the NIR beam. The foil is held by a glass plate, similar to [3]. This allows the outermost part of the NIR beam to pass around the filter. The subsequent center-hole mirror geometrically separates the transmitted donut-shaped NIR from the central XUV beam. The XUV propagates through the hole and the NIR is reflected from the backside of the mirror. The OPA beam hits the center-hole mirror on the front side. While most of the OPA beam is reflected, a small fraction passes through the hole and can be used together with the residual NIR for the active phase stabilization.

The two beams are focused into a BBO crystal, which is optimized for second order harmonic generation of the OPA wavelengths. The spectra of the NIR and the second harmonic of the OPA overlap sufficiently over a sizeable fraction of the OPA tuning range. A narrow band-pass filter with a center wavelength of 780 nm (FWHM = 10 ± 2 nm) is placed behind the BBO. The interference pattern resulting from the NIR and the OPA second harmonic is recorded with a CMOS camera placed behind the filter. While a small change of the angle between the two interfering beams on the camera can cause a change of the spatial frequency of the fringes, it does not affect the value of their phase. The phase is only affected by changes of the individual interferometer path lengths, which is exactly what is to be stabilized by our scheme. It is important to note that our system stabilizes the relative phase of the two pulses, rather than just their envelopes. This is very important for phase-sensitive attosecond pump-probe measurements.

Further, it would also be possible to record the spectral interference with a spectrometer instead of the spatial fringes with the CMOS camera. Such a spectrometer, however, would need sufficient resolution to resolve the interference fringes across the entire delay range to be scanned. Furthermore, a spectrometer adds additional cost compared to a CMOS camera and a band-pass filter.

However, our approach of stabilizing the NIR and OPA pulses without the help of an auxiliary laser presents some challenges and limitations:

(i) CEP-stability of both pulses, NIR and OPA, is required for observing stable interference fringes.

(ii) The interference signal on the camera occurs only if the two spectrally filtered pulses are within a coherence length of each other, which limits the delay window for stabilization.

With the narrow band-pass filter used in our present implementation, we measured interference fringes during a pump-probe delay window of roughly 100 fs. This corresponds to about 19 optical cycles of the OPA pulse. In addition to the intrinsic limitations listed above, we observed a setup-specific issue, which had to be taken into account. Our design of the laser beam paths implies that when the XUV and OPA pulses temporally overlap at the experimental target, the NIR and OPA pulses going towards the CMOS camera are temporally separated. The reason for this is illustrated in Fig. 2(a). After the HHG process, the NIR and XUV overlap in time. The outer part of the NIR beam passes through the glass mount and is thereby delayed with respect to the HHG radiation. In addition, the NIR reflection on the center-hole mirror, which is coated on the OPA facing side, results in a further delay, as the NIR beam has to cross the mirror substrate twice. As a consequence, in the case of setting the XUV and OPA pulse to temporally overlap in the experimental target, the OPA and NIR pulses reaching the CMOS camera are delayed by about 6.6 ps with respect to each other for our design parameters.

Taking into account that the pulse durations of the NIR and OPA are less than 50 fs, it is necessary to compensate for the accumulated delay to observe interference fringes on the camera while the OPA/XUV pulses overlap at the experimental target. To do so, we use additional delay-compensating optical elements, see Fig. 2(b). A longpass filter (cut-on wavelength: 1000 nm) and a pair of motorized fused silica wedges are installed and vertically aligned so that the OPA propagates through them while the NIR is partly blocked by the filter. The additional glass delays the OPA with respect to the NIR. Hence, by tuning the amount of glass in the beam path, the simultaneous overlap in the experimental target and on the CMOS camera can be achieved. The wedges could in principle also be used to extend the delay range that can be stabilized beyond the limit mentioned above.

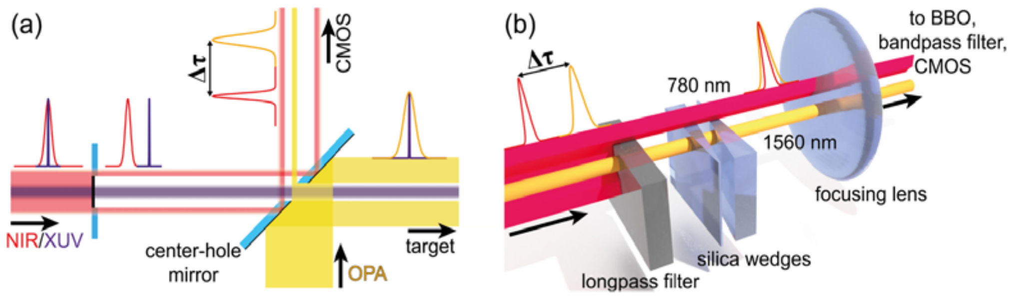


Fig. 2. Delay compensation. (a) NIR (red), XUV (violet) and OPA (yellow) beam paths. When the XUV and OPA pulses overlap in time in the experimental target, the NIR is delayed compared to the OPA pulse on the CMOS camera by about $\Delta\tau = 6.6$ ps. (b) Additional optics installed before the camera to compensate for the acquired delay. The temporally overlapping pulses are finally focused with a lens into a BBO crystal for second order harmonic generation of the OPA beam, followed by a narrow band-pass filter (center wavelength: 780 nm, FWHM: 10 ± 2 nm) and a CMOS camera.

## 4. Active interferometric stabilization (AIS) algorithm

As mentioned above, CEP stability is required to observe stable interference fringes. The CEP stabilization of the Ti:sapphire amplifier system consists of two loops. The fast loop acts on the oscillator and locks the carrier-envelope offset frequency to $1/4$ of the repetition rate, which translates to a constant CEP $\varphi_{NIR}^{CEP}$ after the pulse-picker of the amplifier. The slow loop compensates long-term CEP drifts by adjusting a wedged glass element in the amplifier's bulk glass stretcher. Since the OPA seed is produced via white-light generation, the CEP of the OPA signal is equal to the one of the NIR pulse, $\varphi_{NIR}^{CEP} = \varphi_{OPA}^{CEP}$. At the same time, the frequency-doubled signal of the OPA used to produce interference fringes on the camera for active phase stabilization carries twice that offset, $\varphi_{SH}^{CEP} = 2\varphi_{NIR}^{CEP} + \frac{\pi}{2}$. The $\frac{\pi}{2}$ results from the second harmonic (SH) generation. As a result, the interference patterns forming on the camera are directly influenced when tuning $\varphi_{NIR}^{CEP}$:

$$\begin{aligned}\Delta\varphi &= \varphi_{SH} - \varphi_{NIR} \\ &= \left[\varphi_{SH}^{CEP} - \varphi_{NIR}^{CEP}\right] + \Delta\varphi_{path}, \\ &= \varphi_{NIR}^{CEP} + \frac{\pi}{2} + \Delta\varphi_{path}\end{aligned} \tag{1}$$

where $\Delta\varphi$ is the phase difference between the NIR and the second harmonic of the OPA detected at the CMOS camera. Thus, $\Delta\varphi$ includes the phase difference due to the path difference in the interferometer, $\Delta\varphi_{path}$, as well as the CEP of the NIR, $\varphi_{NIR}^{CEP}$. Since the feedback of the AIS only acts on $\Delta\varphi_{path}$ while still detecting $\varphi_{NIR}^{CEP}$, it is crucial to minimize any CEP fluctuations. With our system, the CEP of the NIR could be stabilized to a rms value of <0.18 rad, which corresponds to 75 as. Without having the CEP stabilization running, no interference fringes can be observed on the camera.

Figure 3 shows the schematic of the home-built proportional-integral-derivative (PID) software to stabilize the relative phase $\Delta\varphi$ between the NIR and OPA pulses. The stabilization loop consists of the phase extraction algorithm and the PID-controlled feedback to the piezo-driven delay stage and runs at 431 Hz, limited by the camera readout rate. This frequency is significantly higher than the dominating mechanical instabilities of the setup (<40 Hz), as was confirmed with an independent accelerometer measurement. The high acquisition rate allows for tracking the delay also in the event of occasional fast, high-amplitude mechanical perturbations. Given the short path length and the common path of the NIR and OPA beams between the center-hole mirror and the camera, we assume the noise contributions acquired in this part of the setup to be negligible compared to the fluctuations from the 23 m long interferometer arms. This assumption is supported by the attosecond streaking experiment reported in section 5.

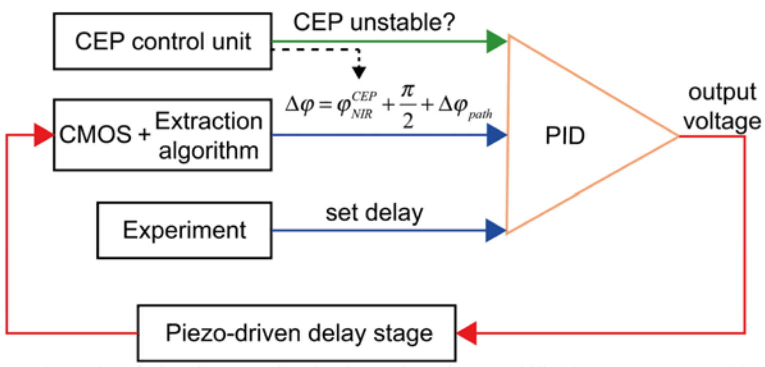


Fig. 3. Schematic of signal processing in the active phase stabilization system. The black dashed arrow indicates that the CEP stabilization of the NIR beam affects the interference fringes observed with the CMOS camera.

From time to time, the CEP stabilization is interrupted, e.g. when the oscillator loop moves the intra-cavity glass wedges that are used for coarse adjustment of the CEP offset. The resulting very fast CEP jumps cannot be distinguished from changes in the propagation phase $\Delta\varphi_{path}$ by our detection system and ultimately lead to loss of the phase tracking. To overcome this issue, an additional logical signal, shown as the green arrow in Fig. 3, is implemented in the PID software. It interrupts the phase acquisition from the CMOS while the CEP is unstable. The last measured phase is kept for subsequent tracking once CEP stability is regained.

## 5. Measurement

To demonstrate the stability as well as the importance of the active phase correction system, we performed a series of photoelectron streaking measurements. Photoelectron streaking is a commonly used technique for studying attosecond dynamics [8]. In a streaking experiment, a single attosecond pulse (SAP) ionizes a gas target (here, neon). The spectrum of the used SAP is shown in Fig. 4(a). The kinetic energy distribution of the electrons photo-emitted from the gas atoms corresponds to the spectrum of the SAP minus the ionization energy ($E_{Ne}$ = 21.56 eV). We use a time-of-flight spectrometer to detect the electron kinetic energies. During the overlap of the XUV and OPA pulses, the energy distribution is additionally shifted by the vector potential of the OPA pulse and thus oscillates with the pump-probe delay. The oscillation frequency corresponds to the optical frequency of the OPA beam.

Figure 4(b) illustrates a typical streaking trace recorded around the pump-probe overlap. To the best of our knowledge, this is the first streaking demonstration involving two different IR colors for HHG and to streak the photo-emitted electrons. The red curve in Fig. 4(b) indicates the center of mass. Phase instabilities and temporal drifts between the pump-probe pulses are directly imprinted in a streaking trace. Consequently, this technique is a good test for the reliability of the phase stabilization system.

We recorded a set of three streaking traces measured in sequence, with an acquisition time of about 10 minutes per trace followed by a 2-3 minutes break between two consecutive runs. Figure 4(c) compares the center-of-mass traces extracted from the three data sets. In addition, we plot in Fig. 4(d) the correction applied by the stabilization system during this measurement period.

The correction between the first and the last scan amounts to almost 8 fs, which is significantly more than the oscillation period at the OPA wavelength ($\tau \approx 5.2$ fs). The rms error between the set and the in-loop delay, extracted with the AIS software, amounted to about 450 as for the proof-of-principle measurement. Further, we performed an additional stability measurement, where the pump-probe delay has been kept at a fixed value for 30 min. Here, a rms value below 300 as has been extracted while the stabilization loop had to compensate for a drift on the order of 20 fs. Thus, the reported 450 as represent the in-loop delay stability achievable under dynamic operation of the system.

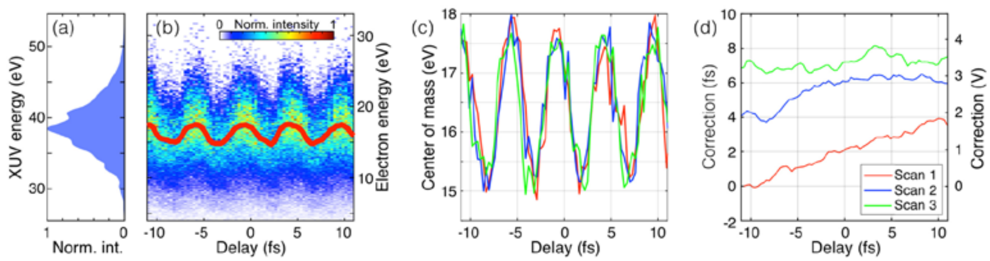


Fig. 4. Attosecond streaking experiment as a proof-of-principle demonstration. (a) Normalized XUV spectrum of the SAP. (b) Typical streaking trace of the photo-emitted electrons recorded with a time-of-flight spectrometer. The red line marks the center of mass of the energy distribution at each pump-probe delay. (c) Extracted center-of-mass traces from three delay scans recorded in sequence. (d) Correction to the pump-probe delay applied by the stabilization system (in fs and Volt).

Our phase acquisition software could in principle also be used for only tracking the phase without providing a feedback to the piezo that controls the delay. This could potentially reduce noise contributions induced by the feedback loop. The tracked fluctuations could then be used as a correction in the post-processing of the recorded data. In our case we observed however that even after warming up the system for several hours, delay drifts of several femtosecond per hour and thus on the order of the pump-probe overlap occur. Since a typical attosecond pump-probe experiment can take up to several hours, an active feedback is therefore preferred in our system. Furthermore, the post-correction cannot be applied if the measurement involves long exposures, i.e. if the exposure is slower than the correction frequency. In this case, the signal will be averaged over a potentially large range of relative phases and post-processing will not be able to recover delay-resolution in the pump-probe signal.

## 6. Conclusion

To conclude, we demonstrated active phase stabilization of an attosecond pump-probe beamline involving two IR colors. In our setup, the output of a Ti:sapphire amplifier is divided in two. One part pumps an OPA while the other one generates the attosecond XUV pulse. The signal beam from the OPA system is later recombined with the attosecond pulse to perform pump-probe measurements. The pump-probe interferometer from the first beam splitter to the recombination optics has a total arm length of about 23 m, with most of the beam path in open air.

Our system directly stabilizes the relative phase between the two colors propagating along the different interferometer arms. The direct phase sensitivity would not be possible if an auxiliary cw laser was used for the stabilization. In our approach, a fraction of the HHG driving beam is focused together with a part of the OPA beam into a BBO crystal followed by a camera. The overlapping spectral portion of the Ti:sapphire pulse and the second harmonic of the OPA is extracted with a narrow-bandwidth bandpass filter and produces an interference pattern on the camera.

With a home-built PID feedback algorithm, the interference fringes are stabilized and with it the relative phase of the involved pulses. We demonstrate delay stabilization between two IR colors to within 450 as rms. To prove the long-term sub-femtosecond stability of our system, we recorded a series of attosecond streaking traces. This experiment also illustrates that active stabilization is essential to resolve sub-femtosecond dynamics with a beamline involving two IR colors accurately. Without active stabilization, drifts of several femtosecond per hour occur.

## Funding

NCCR MUST, funded by the Swiss National Science Foundation (SNSF); ETH Zurich Postdoctoral Fellowship Program.

## References

1. M. Chini, H. Mashiko, H. Wang, S. Chen, C. Yun, S. Scott, S. Gilbertson, and Z. Chang, "Delay control in attosecond pump-probe experiments," Opt. Express **17**(24), 21459–21464 (2009).
2. M. Huppert, I. Jordan, and H. J. Wörner, "Attosecond beamline with actively stabilized and spatially separated beam paths," Rev. Sci. Instrum. **86**(12), 123106 (2015).
3. M. Sabbar, S. Heuser, R. Boge, M. Lucchini, L. Gallmann, C. Cirelli, and U. Keller, "Combining attosecond XUV pulses with coincidence spectroscopy," Rev. Sci. Instrum. **85**(10), 103113 (2014).
4. R. Locher, M. Lucchini, J. Herrmann, M. Sabbar, M. Weger, A. Ludwig, L. Castiglioni, M. Greif, M. Hengsberger, L. Gallmann, and U. Keller, "Versatile attosecond beamline in a two-foci configuration for simultaneous time-resolved measurements," Rev. Sci. Instrum. **85**(1), 013113 (2014).
5. G. Sansone, E. Benedetti, F. Calegari, C. Vozzi, L. Avaldi, R. Flammini, L. Poletto, P. Villoresi, C. Altucci, R. Velotta, S. Stagira, S. De Silvestri, and M. Nisoli, "Isolated single-cycle attosecond pulses," Science **314**(5798), 443–446 (2006).
6. M. Volkov, S. A. Sato, F. Schlaepfer, L. Kasmi, N. Hartmann, M. Lucchini, L. Gallmann, A. Rubio, and U. Keller, "Attosecond screening dynamics mediated by electron localization in transition metals," Nat. Phys. 10.1038/s41567-019-0602-9 (2019).
7. Y. Pertot, C. Schmidt, M. Matthews, A. Chauvet, M. Huppert, V. Svoboda, A. von Conta, A. Tehlar, D. Baykusheva, J.-P. Wolf, and H. J. Wörner, "Time-resolved x-ray absorption spectroscopy with a water window high-harmonic source," Science **355**(6322), 264–267 (2017).
8. J. Itatani, F. Quéré, G. L. Yudin, M. Y. Ivanov, F. Krausz, and P. B. Corkum, "Attosecond streak camera," Phys. Rev. Lett. **88**(17), 173903 (2002).
9. A. L. Cavalieri, N. Müller, T. Uphues, V. S. Yakovlev, A. Baltuška, B. Horvath, B. Schmidt, L. Blümel, R. Holzwarth, S. Hendel, M. Drescher, U. Kleineberg, P. M. Echenique, R. Kienberger, F. Krausz, and U. Heinzmann, "Attosecond spectroscopy in condensed matter," Nature **449**(7165), 1029–1032 (2007).
10. M. Schultze, M. Fiess, N. Karpowicz, J. Gagnon, M. Korbman, M. Hofstetter, S. Neppl, A. L. Cavalieri, Y. Komninos, T. Mercouris, C. A. Nicolaides, R. Pazourek, S. Nagele, J. Feist, J. Burgdörfer, A. M. Azzeer, R. Ernstorfer, R. Kienberger, U. Kleineberg, E. Goulielmakis, F. Krausz, and V. S. Yakovlev, "Delay in photoemission," Science **328**(5986), 1658–1662 (2010).
11. M. Ossiander, F. Siegrist, V. Shirvanyan, R. Pazourek, A. Sommer, T. Latka, A. Guggenmos, S. Nagele, J. Feist, J. Burgdörfer, R. Kienberger, and M. Schultze, "Attosecond correlation dynamics," Nat. Phys. **13**(3), 280–285 (2017).
12. M. Sabbar, S. Heuser, R. Boge, M. Lucchini, T. Carette, E. Lindroth, L. Gallmann, C. Cirelli, and U. Keller, "Resonance Effects in Photoemission Time Delays," Phys. Rev. Lett. **115**(13), 133001 (2015).
13. T. Otobe, Y. Shinohara, S. A. Sato, and K. Yabana, "Femtosecond time-resolved dynamical Franz-Keldysh effect," Phys. Rev. B **93**(4), 045124 (2016).
14. M. Lucchini, S. A. Sato, A. Ludwig, J. Herrmann, M. Volkov, L. Kasmi, Y. Shinohara, K. Yabana, L. Gallmann, and U. Keller, "Attosecond dynamical Franz-Keldysh effect in polycrystalline diamond," Science **353**(6302), 916–919 (2016).
15. H. R. Telle, G. Steinmeyer, A. E. Dunlop, J. Stenger, D. H. Sutter, and U. Keller, "Carrier-envelope offset phase control: A novel concept for absolute optical frequency measurement and untrashort pulse generation," Appl. Phys. B Lasers Opt. **69**(4), 327–332 (1999).
16. W. Liu and S. Chin, "Direct measurement of the critical power of femtosecond Ti:sapphire laser pulse in air," Opt. Express **13**(15), 5750–5755 (2005).